Journal of Alloys and Compounds 591 (2014) 286–292

Contents lists available at ScienceDirect

Journal of Alloys and Compounds

journal homepage: www.elsevier.com/locate/jalcom

Nd_2O_3:Gd^{3+} nanocrystalline phosphor: γ-Induced thermoluminescence, EPR and structural properties

B. Umesh [a], H. Nagabhushana [b,*], S.C. Sharma [c], B. Eraiah [d], N. Dhananjaya [e], B.M. Nagabhushana [f], J.L. Rao [g], R.P.S. Chakradhar [h]

[a] Department of Humanities, PVP Polytechnic, Dr. AIT Campus, Bangalore 560 056, India
[b] Prof C.N.R. Rao. Centre for Advanced Materials, Tumkur University, Tumkur 572 103, India
[c] Department of Mechanical Engineering, BMS Institute of Technology, Yelahanka, Bangalore 560 064, India
[d] Department of Physics, Bangalore University, Bangalore 560 056, India
[e] Department of Physics, BMS Institute of Technology, Yelahanka, Bangalore 560 064, India
[f] Department of Chemistry, M.S. Ramaiah Institute of Technology, Bangalore 560 054, India
[g] Department of Physics, Sri Venkateswara University, Tirupati 517 502, India
[h] CSIR-National Aerospace Laboratories, Bangalore 560 017, India

ARTICLE INFO

Article history:
Received 16 August 2013
Received in revised form 2 December 2013
Accepted 6 December 2013
Available online 16 December 2013

Keywords:
Phosphor
Nanocrystallite
Thermoluminescence
Trap parameters
Combustion synthesis

ABSTRACT

Preparation of nanocrystalline Nd_2O_3:Gd^{3+} (2 mol%) phosphor was prepared by propellant combustion route at low temperature. Powder X-ray diffraction (PXRD), transmission electron microscopy (TEM) and scanning electron microscopy (SEM) techniques were used to study the structural and morphological features. A and C type hexagonal phase of Nd_2O_3 was obtained in as-formed and calcined product at 900 °C for 3 h. SEM images show the product was highly porous, agglomerated and irregular shaped particles. The average crystallite size estimated from Scherrer's and W–H plots were found to be in the range ~20–50 nm. Combination of F_g and (F_g + E_g) modes were observed from Raman studies. A single TL glow peak at 409 K was recorded at a warming rate 5 °C s^{-1}. TL response as a function of γ-irradiation showed linear response up to 1.6 kGy and later it followed exponential growth. The phosphor show simple glow curve structure with less fading over a period of 30 days. Trap parameters were estimated from Chen's peak shape method. The activation energy (E) and frequency factor (s) was found to in the range 1.377–2.934 eV and 2.01×10^{11}–8.70×10^{22} Hz respectively.

1. Introduction

Recently, rare earth and transition metal ions doped oxide hosts find wide range of applications including luminescent materials, catalysts, photonic applications, displays, thermoluminescence dosimetry [1–4], etc. Oxide host phosphors were commonly synthesized by numerous methods namely sol–gel, hydrothermal, co-precipitation, combustion, solid-state method [5–8], etc. Among them solution combustion (SC) method was highly capable of producing nano synthesized products with large surface area, nano size, high purity, large production, etc. This technique was a robust, inexpensive and exothermic reaction which undergoes self-sustaining, no extra heating was required. Further, size, shape can be tuned by varying the parameters namely fuel, fuel/oxidizer (F/O) ratio, water content, etc. [9].

Presently, synthesis of nanocrystalline materials with low temperature and short reaction time were highly desirable for phosphor industry. In the present work Nd_2O_3:Gd^{3+} (2 mol%) nanophosphor was synthesized by low temperature solution combustion method using ODH as fuel. The final product was subjected to structural, morphological, luminescence and EPR studies.

2. Experimental

High purity neodymium nitrate ($Nd(NO_3)_3{\cdot}6H_2O$) and gadolinium nitrate ($Gd(NO_3)_3{\cdot}6H_2O$) were used as a starting materials procured from sigma aldrich without further purification. 2 mol% Gd doped Nd_2O_3 nanocrystalline phosphor was prepared by taking stoichiometric amounts of $Nd(NO_3)_3{\cdot}6H_2O$, $Gd(NO_3)_3{\cdot}6H_2O$ and oxalyldihydrazide ($C_2H_6N_4O_2$; ODH) as a fuel. The corresponding nitrates and ODH was mixed thoroughly in a cylindrical Pyrex dish using magnetic stirrer for ~5 min. Thereafter the cylindrical Pyrex dish containing heterogeneous mixture was placed exactly at the center of the pre-heated muffle furnace maintained at 400 ± 10 °C. The mixture undergoes thermal dehydration and ignition with liberation of large number of gaseous products. The flame temperature was measured using optical pyrometer which was placed inside the muffle furnace. Finally the voluminous and foamy porous product was obtained. Further the as-formed product was calcined for ~900 °C for 3 h and used for structural characterization and luminescence studies. Theoretical equation assuming the complete combustion of the redox mixture used for the synthesis of Nd_2O_3 phosphor may be written as

$$2Nd(NO_3)_3 + 3C_2H_6N_4O_2 \rightarrow Nd_2O_3 + 6CO_2 + 9H_2O + 9N_2 \quad (1)$$

* Corresponding author. Tel.: +91 9945954010 (mobile).
E-mail address: bhushanvlc@gmail.com (H. Nagabhushana).

0925-8388/$ - see front matter © 2013 Elsevier B.V. All rights reserved.
http://dx.doi.org/10.1016/j.jallcom.2013.12.052

2.1. Instrument used

The structural and morphological characterization of the product was investigated by powder X-ray diffraction (PXRD), scanning electron microscopy (SEM) and transmission electron microscopy (TEM). PXRD studies were carried out in $2\theta = 10–80°$ range using Shimadzu X-ray diffractometer with Cu Kα radiation. TEM analysis was done using TECNAI F-30 model. For TEM analysis the crush and float technique was used, where powder was crushed with a small pestle mortar-in methanol, ultrasonicated and drop casted on a 300 mesh lacey carbon grid. SEM analysis was done using Hitachi Tabletop SEM without gold coating. Raman measurement was performed using Renishaw In via Raman spectrometer with 633 nm He–Cd laser equipped with 50x objective optical microscope with a laser spot of 2 μm in diameter. FT-IR studies were performed using Perkin Elmer Spectrometer (Spectrum 1000) with KBr pellets. The UV–Vis absorption of the samples was recorded on SL 159 ELICO UV–Vis Spectrophotometer. EPR spectra was recorded on an EPR spectrometer (JEOL-FE1X) operating in the X-band frequencies with a field modulation of 100 kHz with microwave frequency of 9.205 GHz. TL measurements were recorded on a Nucleonix TL reader at RT by taking equal quantity of phosphor each time. TL measurements were done with in a time gap of 24 h after γ irradiation. For defects creation, γ-irradiation in the dose range 0.23–2.05 kGy was performed on ^{60}Co source. Photoluminescence (PL) was performed on a Horiba Spectrofluoremeter (Model Flurolog-3) equipped with 150 W Xenon lamp as an excitation source.

3. Results and discussion

3.1. Powder X-ray diffraction

Fig. 1(a and b) shows the PXRD patterns of as-formed and calcined Nd_2O_3:Gd^{3+} (2 mol%) nanophosphor at 900 °C for 3 h. The diffraction patterns of as-formed and calcined product was well matched with a hexagonal A and C type (JCPDS Card No. 83–1353) Nd_2O_3. Further, the intensity of the diffraction peaks were found to be higher in calcined samples, due to increase of crystallinity. The line breading of the highest peak ($2\theta = 31.5°$) was used to calculate the average crystallite size of the phosphor using Scherrer's formula [10] $d = n\lambda/\beta \cos\theta$, where d, average crystallite size; β, FWHM; λ, wave length of X-ray used. The crystallite size was found to be in the range of 20–50 nm. The strain and crystallite size was estimated from W–H plots method [11] using the relation $\beta_{hkl}\cos\theta_{hkl} = \frac{k\lambda}{d} + 2\varepsilon\sin\theta_{hkl}$.The plot of $\beta\cos\theta$ along y-axis and $4\sin\theta$ along x-axis was shown in Fig. 2. The slope of the line gives the strain and the intercept of the same line gives the crystallite size. The values of the crystallite size and strain for as-formed and calcined products obtained were given Table 1. It was observed that strain present in as-formed sample was found to be higher when compared to Gd^{3+} doped Nd_2O_3. This increase in strain may cause the shifting and broadening of the PXRD peaks shown in inset of Fig. 1. The crystallite size anticipated from W–H plots was to some extent higher than those expected using Scherrer's method. The discrepancy in the values was due to the fact that in Scherer's method, the strain component was assumed to be zero and obtained broadening of diffraction peak was considered as a result of reducing grain size only [12].

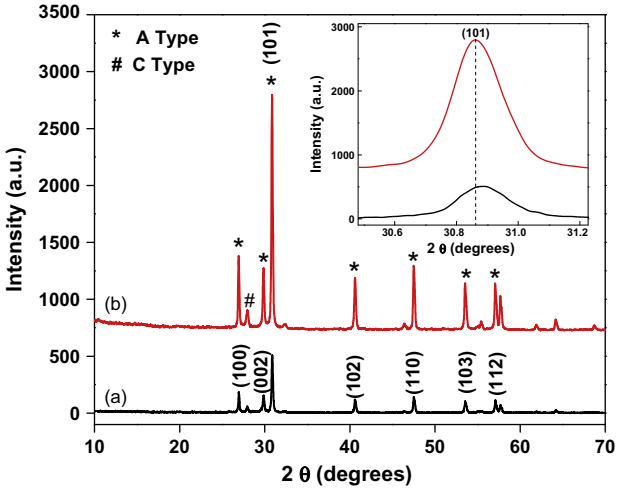

Fig. 1. PXRD patterns of Nd_2O_3:Gd^{3+} nanophosphor (a) as- formed(b) calcined at 900 °C for 3 h.

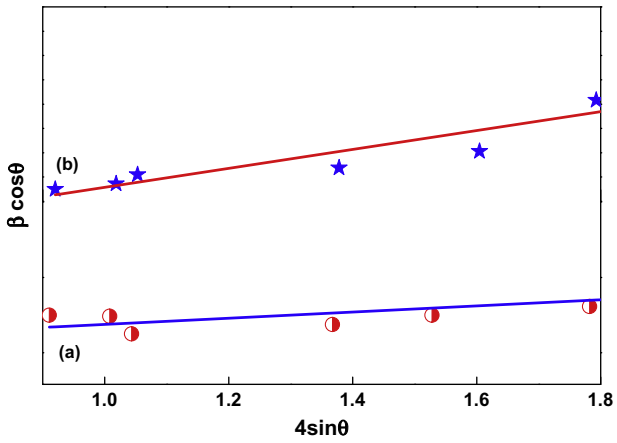

Fig. 2. W–H plot of Nd_2O_3:Gd^{3+} nanophosphor (a) as-formed and (b) calcined at 900 °C for 3 h.

Table 1
Various estimated parameters (particle size, strain and band gap values) of Nd_2O_3:Gd^{3+} phosphors calcined at 900 °C.

Nd_2O_3: Gd^{3+} (2 mol%)	Crystallite size (nm)		Strain ($\times10^{-4}$)	Band gap (eV)
	Scherer's method	W–H method		
As-formed	24.86	27.37	7.33	5.20
Calcined at 900 °C for 3 h	39.22	47.46	3.88	5.50

3.2. Morphological studies

Fig. 3(a and b) depicts the SEM micrographs of as-formed and calcined Nd_2O_3:Gd^{3+} nanophosphors. It was evident from SEM images; the product was highly porous in nature, crispy, large voids and agglomerated particles. The porous nature was mainly attributed to the large amount of gases escaping from the reaction mixture during combustion [13]. Fig. 3(c) shows the transmission electron microscopy (TEM) image of calcined Nd_2O_3:Gd^{3+} (2 mol%) at 900 °C for 3 h. The average particle size was found to be in the range ~50–350 nm. To examine the crystalline nature and atomic structure information of the phosphor, high resolution transmission electron microscopic (HRTEM) was studied (Fig. 3(d)). A clear atomic lattice fringes indicate highly uniform structure and dislocation free. The lattice space (d) corresponding to (1 0 1) plane was calculated and found to be ~3.6 nm. In order to estimate the atomic and molecular weight of the compound, EDXA was studied and shown in Fig. 3(e).

3.3. Fourier transform infrared spectroscopy (FTIR)

Fig. 4 shows the FTIR spectra of as-formed and calcined Nd_2O_3:-Gd^{3+} (2 mol%) phosphor at 900 °C for 3 h. The characteristic metal–oxygen (Nd–O) vibrations were observed at 407 and 670 cm^{-1} [14]. The sharp peak at ~3615 cm^{-1} was due to metal hydroxide (M–OH) peak. The bands between 3300–3700 cm^{-1} were due to the (O–H) vibration of H_2O absorbed by Nd_2O_3 phosphor. The

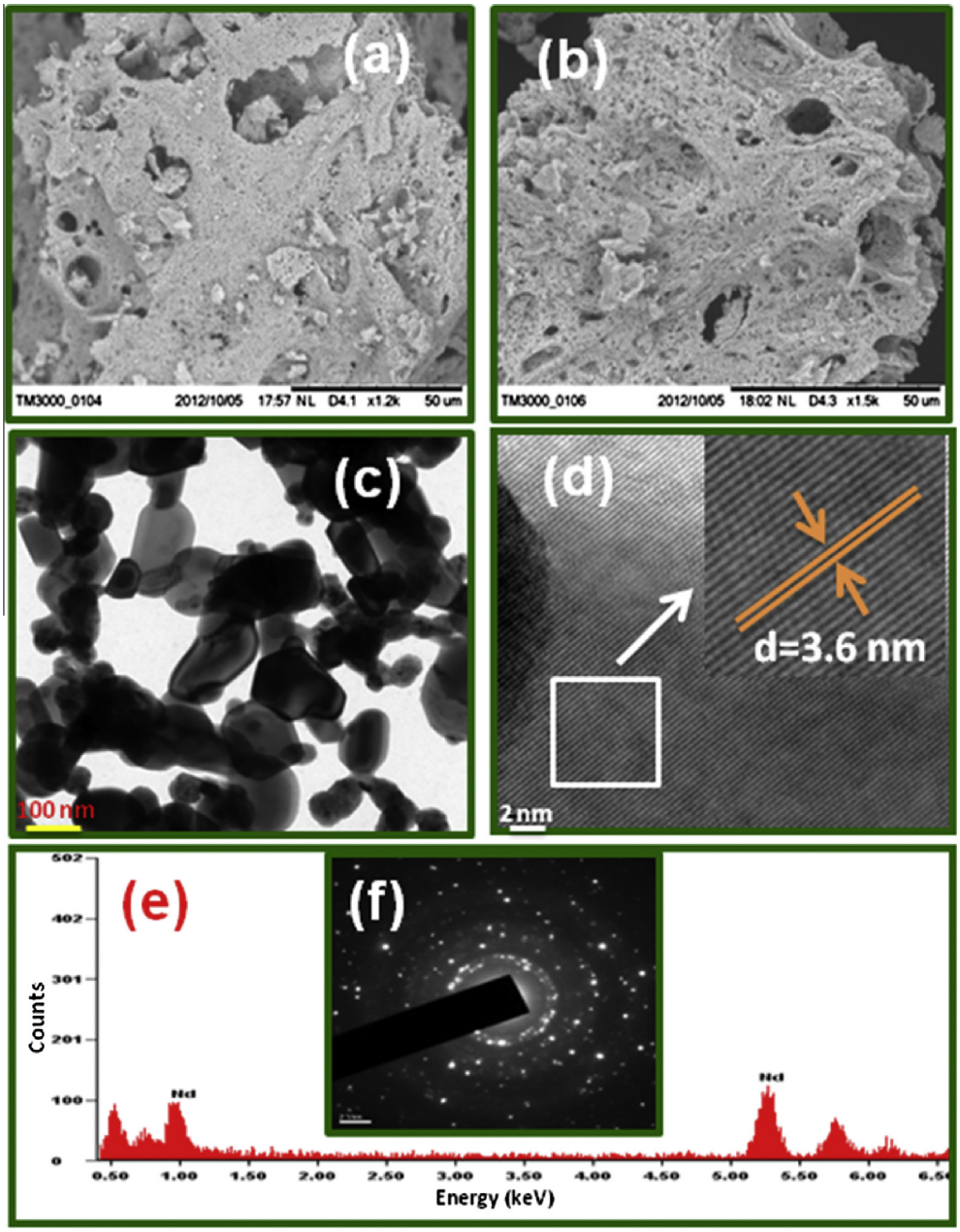

Fig. 3. (a) SEM, images of Nd_2O_3:Gd^{3+} nanophosphor as formed and (b) calcined at 900 °C for 3 h, (c) TEM, (d) SAED and (e) EDAX.

peaks observed at 1374 and 1586 cm^{-1} were due to CO_3^{2-} anion group. We believe that the possible source of the carbonyl group was from oxalyl dihydrazide fuel used for the combustion synthesis [15].

3.4. UV–Visible absorption and band gap measurement (E_g)

The UV–Visible absorption spectra of as-formed and calcined Nd_2O_3:Gd^{3+} at 900 °C for 3 h recorded in the wavelength range 200–800 nm was shown in Fig. 5(a and b). A broad absorption band was observed in as-formed product at 256 nm. However, in calcined Gd^{3+} doped Nd_2O_3, a prominent absorption peaks were recorded in the range 530–600 nm (inset Fig. 5). The absorption peak at 246 nm was due to photo excitation of electron from valance band to conduction band [16]. Whereas, the peaks recorded in the range 530–600 nm were due oxygen vacancies [17]. The energy gap (E_g) of as-formed and calcined sample was estimated using Tauc's relation by plotting $(\alpha h\nu)^2$ vs photon energy (Fig. 6). The E_g values of as-formed and calcined sample were found to be 5.2 and 5.5 eV respectively. The E_g value for the calcined sample was well matched with reported literature [18]. Further, the E_g value was found to be lesser in as-formed sample when compared to calcined sample. This might be due to presence of large number of defects namely surface defects, oxygen vacancies, distortion, lattice strain, etc. However, in calcined sample, the defects were completely nullified and the structure was more ordered. The variation of E_g values may be due to method of preparation, amorphous or crystalline nature of the product.

3.5. Raman studies

Raman spectrum of Nd_2O_3:Gd^{3+} (2 mol%) excited at 633 nm laser light was recorded in the range 50–3000 cm^{-1} (Fig. 7). A sharp and intense Raman peaks were recorded at ~68, 151, 346, 438, 1835, 1936, 1992, 2064 and 2408 cm^{-1}. The intense peaks observed in both lower and higher wavenumber side were mainly

Table 2
Estimated kinetic parameters of 900 °C calcined Nd_2O_3:Gd^{3+} nanophosphor by Chen's peak shape method.

Dose (kGy)	Peak	T_m (K)	b (μ_g)	Activation energy (eV)				Frequency factor (s^{-1})
				E_τ	E_δ	E_ω	E_{ave}	
0.23	1	399	2(0.49)	1.346	1.403	1.381	1.377	2.01E+11
	2	412	2(0.51)	2.53	2.434	2.495	2.486	3.50E+19
0.69	1	399	2(0.50)	1.359	1.409	1.391	1.386	2.40E+11
	2	413	2(0.48)	2.256	2.242	2.265	2.254	5.98E+17
1.14	1	399	2(0.48)	1.923	1.935	1.942	1.933	4.53E+15
	2	412	2(0.49)	2.769	2.696	2.753	2.739	2.83E+21
1.60	1	398	2(0.48)	1.887	1.902	1.907	1.899	2.53E+15
	2	413	2(0.49)	2.575	2.523	2.567	2.555	1.11E+20
2.05	1	398	2(0.49)	2.043	2.037	2.053	2.044	3.41E+16
	2	412	2(0.49)	2.982	2.873	2.948	2.934	8.70E+22

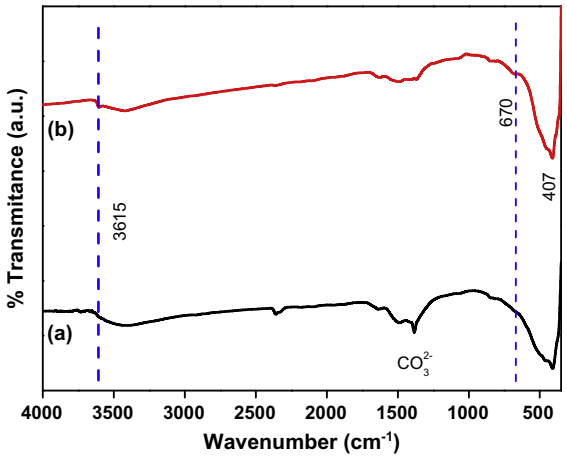

Fig. 4. FTIR spectra of Nd_2O_3:Gd^{3+} nanophosphor (a) as-formed and (b) calcined at 900 °C for 3 h.

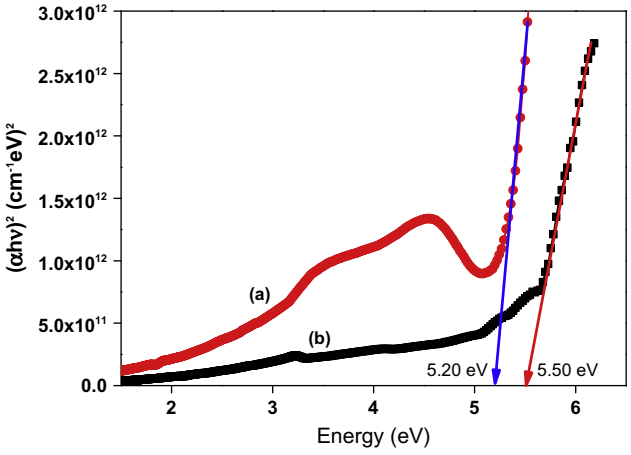

Fig. 6. Band gap of Nd_2O_3:Gd^{3+} nanophosphor (a) as-formed and (b) calcined at 900 °C for 3 h.

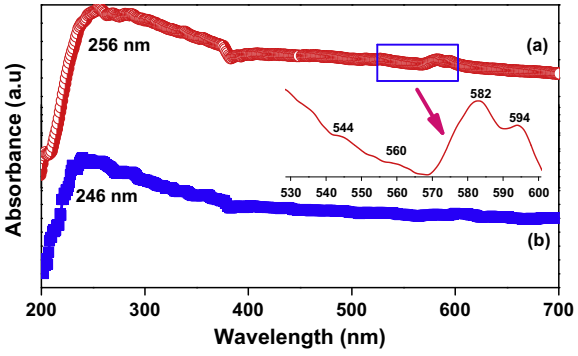

Fig. 5. UV–Vis spectra of Nd_2O_3:Gd^{3+} nanophosphor (a) as-formed and (b) calcined at 900 °C for 3 h.

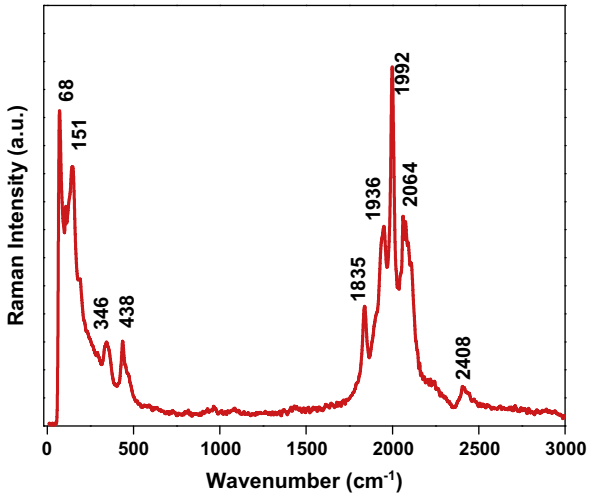

Fig. 7. Raman spectra of Nd_2O_3:Gd^{3+}nanophosphor calcined at 900 °C for 3 h.

attributed to F_g and combination of $F_g + E_g$ modes respectively [19]. The optical and acoustical modes represented in rare earth oxides were given by

$$\Gamma_{op} = 4A_g + 4E_g + 14F_g + 5A_{24} + 5E_4 + 16F_4 \quad (2)$$

$$\Gamma_{ac} = F_4 \quad (3)$$

where A_g. E_g, F_g; Raman active, F_4; IR active and A_{24} and E_4 were inactive. In C type Nd_2O_3, structure totally 22 Raman lines were predicted [20]. It should be noted that none of the Raman spectra show the expected number of optical/acoustical bands. In Y_2O_3 and Sc_2O_3 exhibits 14 and 16 bands which were less as expected from factor group analysis. Further, it was noted that similar number of Raman peaks were observed in single crystals recorded at low temperature (5 K). This might be due to local stress and a large number of point defects can lead to a lowering symmetry and to the band broadening [21]. Raman modes exhibit blue shift of ~13 cm^{-1} was observed in Gd^{3+} doped samples when compared to as-formed Nd_2O_3 prepared by combustion route. This was mainly attributed to lattice distortion. The vibration peaks becomes much stronger and wider in Gd^{3+} doped sample, indicating more number of oxygen vacancies

created after incorporation Gd^{3+} into the Nd_2O_3 lattice. The reduction in Raman modes and shift was due to size effect. Hence, from the above results it may be concluded that there was a decrease of Raman wavenumber in the case of rare earth sesquioxides when compared to bulk material.

3.6. Photoluminescence (PL) studies

Fig. 8 shows the PL emission spectrum of Nd_2O_3:Gd^{3+} monitoring at 270 nm excitation. The spectrum exhibits a strong and narrow emission line at 308 nm along with weak peaks at 297, 302 and 317 nm. These emission peaks were attributed to the f–f transitions of Gd^{3+} ions [18,22,23].

3.7. Thermoluminescence (TL) studies

Thermoluminescence also known as the thermally stimulated emission of light from an insulator or semiconductor, following the previous absorption of energy from ionizing radiation such as γ-rays, X-rays, β-rays, α-particles, neutrons and energetic ions [24]. It was wide range of advantages over other methods owing to its simplicity of the sample readout, small size, portability, lack of electrical power requirements, etc. The large interest in TL as a technique for radiation dosimetry in environmental, personal and clinical applications pushes the research for producing large number of new and high-performance TLD phosphors.

Fig. 9 shows the TL glow curves of Nd_2O_3:Gd^{3+} (2 mol%) nanocrystalline phosphor γ-irradiated in the dose range 0.23–2.05 kGy at a warming rate of 5 °C s^{-1}. A prominent single glow peak at ~409 K was recorded, for all the exposed doses without changing its glow peak structure. Variation of TL glow peak intensity for 409 K with different γ-doses was plotted and shown in Fig. 10. As can be seen from the figure, TL intensity increases linearly with γ-dose up to 1.6 kGy and there after it increases exponentially. The TL intensity was found to be smallest for lower γ-irradiated samples due to creation of lesser defects/traps. However, for higher γ irradiated samples creation of more number of lattice defects/ traps as a result TL intensity increases. The linear behavior of TL intensity from 0.23 to 2.05 kGy dose range was explained based on track interaction model (TIM) [25,26]. According to this model, the number of trap/ luminescence centers created by γ-irradiation in a track mainly depends upon the cross section and the length of track created inside the matrix. As it was well known that in nanostructured materials, the length of the track crated by high energy

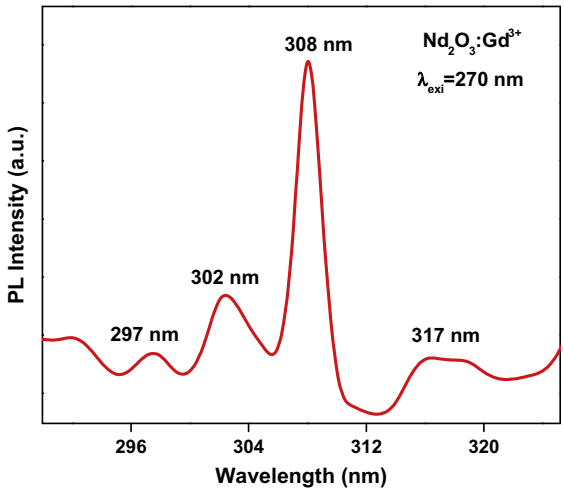

Fig. 8. PL spectra of Nd_2O_3: Gd^{3+} (2 mol%) nanophosphor calcined at 900 °C for 3 h at a excitation wavelength of 270 nm.

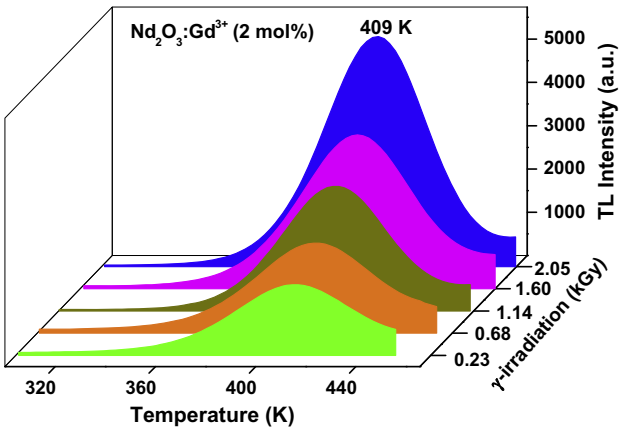

Fig. 9. TL glow curves of Nd_2O_3:Gd^{3+} (2 mol%) nanophosphor irradiated with γ-rays in the dose range 228–2.057 kGy.

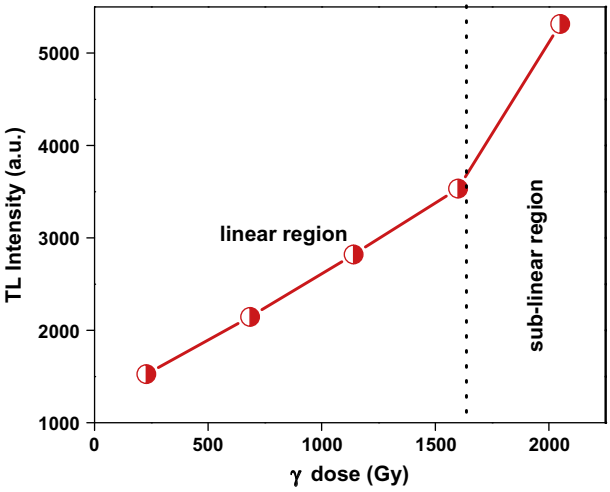

Fig. 10. Variation of TL intensity with γ dose.

radiation (γ) was of the order of few tenths of nanometers (nm). At low doses, there might be present few trapping / luminescence centers (TC). As the γ-dose increase creation of more number of overlapped tracks which may not give extra TL as a result saturation may occur. Thus on increasing higher γ-doses, smaller sized particles which had left out during, irradiation will create more number of trapping/luminescent centers, which intern TL intensity at 409 K glow peak increases. TL glow curves of γ irradiated Nd_2O_3:Ni^{2+} showed two TL peaks at 169 °C and 236 °C at a warming rate of 5 °Cs^{-1}. The TL glow peak intensity at 169 °C increase linearly with dose. The two glow peaks indicated two kinds of trapping centers (shallow/deeper) were created due to γ-irradiation [18]. In the present study, a single shallow trap has been created in the γ dose range 0.23–2.05 kGy.

TL intensity was mainly due to the radiative recombination of previously trapped holes or electrons thermally released from their different trapping sites [27]. Suitable activator and appropriate concentration may enhance the TL intensity. Therefore, the TL glow peak values and its intensity was a characteristic nature of the sample and dopant (TM/RE) ions. The presence of rare earth/transition metal ions may change the TL glow curve structure either enhancing or quenching the TL intensity [28].

TL properties of trivalent Eu^{3+} doped Nd_2O_3 phosphors synthesized by solution combustion technique showed a single glow peak at 426 K in the γ-dose range 100–400 Gy. The TL glow peak intensity with γ-dose follow linear relation, for higher γ-doses the TL

intensity increases exponentially. Further, fading effect was studied nearly 21 days for a test dose of 200 Gy. Strong fading was obtained initially after 4 days; the decay was quite slow and fading stabilities after 21 days.

TLD phosphor generally exhibits one or more peaks when the charge carries (holes or electrons) were released. The dosimetric properties of TL materials largely depend on the kinetic parameters (E, b and s). These parameters will give valuable information about mechanism responsible for the emission in the phosphor. For a good TLD phosphor, a clear knowledge of its kinetic parameters was highly essential. These parameters can be estimated using Chen's set of empirical equations [29]. For the peak shape method by deconvoluting the glow curve by using Glow curve deconvolution (Fig. 11). The peak shape method was generally called Chen's peak method which was used to determine the kinetic parameters of the glow peak of the TL materials. This method was based on the temperatures T_m, T_1 and T_2, where T_m was the peak temperature, while T_1 and T_2 were temperatures at half the intensity on the ascending and descending parts of the glow peak respectively. To determine the kinetic parameters the following shape parameters were determined. The total half intensity width $\omega = T_2 - T_1$, the high temperature half width $\delta = T_2 - T_m$ and low temperature half width $\tau = T_m - T_1$, the peak shape method was mainly used to calculate the order of kinetics. Order of kinetics was evaluated from the symmetry factor (μ_g) of the glow peak; μ_g was calculated from the known peak shape parameters δ and ω

$$\mu_g = \delta/\omega = (T_2 - T_m)/(T_2 - T_1) \tag{4}$$

Order of kinetics depends on the glow peak shape. The value of μ_g for first and second order kinetics was 0.42 and 0.52 respectively.

Chen has provided a plot which gives order of kinetics of the TL process, accordingly to the value of μ_g. Another parameter proposed by Balarian gives the kinetic order as a function of the parameter

$$\gamma = \delta/\tau = (T_2 - T_m)/(T_m - T_1) \tag{5}$$

For the first order kinetics, the Balarian parameter (γ) ranges from 0.7 to 0.8 for second order kinetics it varies from 1.05 to 1.20. Generally in the first order, the process of re-trapping was negligible and the trap should be situated very close to the luminescent centre. The characteristic of the second order peak was wider and more symmetric than the first order peak. For a fixed heating rate, in first order kinetics both peak temperature and shape was independent of the initial trapped electron concentration but in second order,

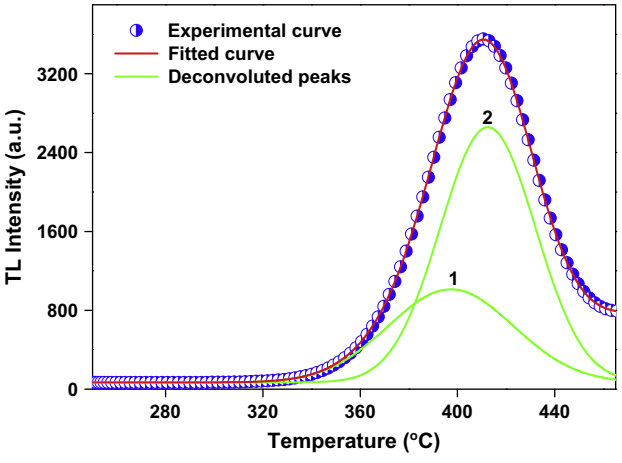

Fig. 11. Glow curve deconvolution of 2 mol% Gd^{3+} doped Nd_2O_3 nanophosphor 1.60 kGy γ-dose at a heating rate of 5 °C s^{-1}.

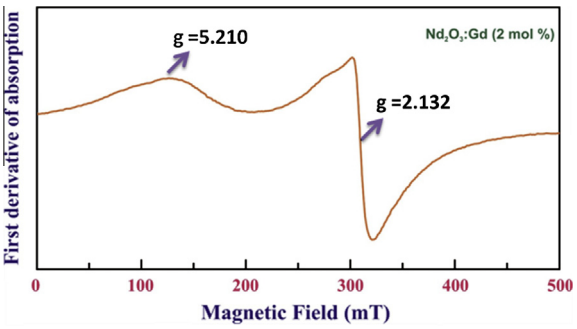

Fig. 12. EPR spectrum of Nd_2O_3: Gd^{3+} (2 mol%) nanophosphor calcined at 900 °C for 3 h.

the peak temperature and shape was strongly dependent on initial trapped charge concentration.

The activation energy (E) was estimated using the general relation for any kinetics which was given by

$$E_\alpha = c_\alpha\left(\frac{kT_m^2}{\alpha}\right) - b_\alpha(2kT_m) \tag{6}$$

where $\alpha = \tau$, δ and ω with $\tau = T_m - T_1$, $\delta = T_2 - T_m$ and $\omega = T_2 - T_1$.

$$C_\tau = 1.51 + 3.0(\mu_g - 0.42), \quad b_\tau = 1.58 + 4.2(\mu_g - 0.42) \tag{7}$$

$$C_\delta = 0.976 + 7.3(\mu_g - 0.42), \quad b_\delta = 0 \tag{8}$$

$$C_\omega = 2.52 + 10.2(\mu_g - 0.42), b_\omega = 1 \tag{9}$$

The frequency factor (s) obtained using the following relation:

$$s = \frac{\beta E}{kT_m^2}\exp\left(\frac{E}{kT_m}\right)[1 + (b-1)\Delta_m]^{-1} \tag{10}$$

where $\Delta = \frac{2kT}{E}$; $\Delta_m = \frac{2kT_m}{E}$ and β; linear heating rate and k; Boltzmann constant (8.6×10^{-5} eV K^{-1}), b; order of kinetics. In this expression 's' depends on T_m, in second order kinetics T_m depends on the absorbed dose. The estimated kinetic parameters of Nd_2O_3:-Ni^{2+}(2 mol%) nanophosphor was given in Table 2.

3.8. Electron paramagnetic resonance (EPR) studies

Fig. 12 depicts the EPR spectrum of Nd_2O_3:Gd^{3+} (2 mol%) nanocrystalline phosphor. The spectrum exhibit two broad EPR signals at $g \approx 2.132$ and $g \approx 5.210$ which were attributed to Gd^{3+} ions. This type of spectrum was aptly labeled as the U-spectrum. An exact analysis of the U-spectrum was complicated by two factors. First, the randomness inherent in disordered systems, results in a broad distribution of crystal field parameters in comparison with that present in polycrystalline powders. Secondly, the EPR absorption curve of the U-spectrum has its maximum near $g \approx 2.0$, a second absorption near $g \approx 6.0$ and a significant amplitude at $g \approx \infty$ (zero field). This indicates that there was a wide range of crystal field strengths where neither the Zeeman interaction nor the crystal field interaction may be realistically treated by perturbation methods.

4. Conclusions

Solution combustion route was used to prepare Nd_2O_3:Gd^{3+} (2 mol%) nanophosphor using ODH as fuel. Mixture of A and C-type of Nd_2O_3 was obtained from PXRD studies. Williamson–Hall (W–H) plots and Scherrer's method was used to estimate the crystallite size and found to be in the range of 20–50 nm. TEM result

further support the nano size of the material. SEM micrographs of the phosphor show highly porous, agglomeration with large voids. The optical band gap of Nd^{3+} doped Nd_2O_3 nanoparticles was 5.5 eV which was higher than the bulk Nd_2O_3 (4.7 eV). This can be attributed to the quantum confinement effect of the nano particles. The broad EPR spectrum show two resonance signals with effective g values at 2.132 and 5.210 were attributed to Gd^{3+} ions. The intense Raman peaks were assigned, to F_g and A_{g+Eg} modes. A single glow peak at 409 K was recorded at a warming rate 5 °C s^{-1}. Variation of TL intensity as a function of γ-irradiation show linear response up to 1.60 kGy and after that it follows exponential growth. The phosphor show simple glow peak structure and less fading over a period of 30 days as a result this might be quite useful in radiation dosimetry. The 409 K glow peak follow second order kinetics (b) and the activation energy (E) & frequency factor (s) varies from 1.377 to 2.934 and 2.01×10^{11} – 8.70×10^{22} Hz respectively.

Acknowledgements

One of the authors (H.N.) thanks to the DST Nano-Mission (Project No. SR/NM/NS-48/2010) New Delhi for sanction of the Project. Prof. S.C. Sharma greatly acknowledge B.M.S. Institutions for constant support.

References

[1] J. Li, G. Lu, B. Xie, Y. Wang, Y. Guo, Y. Guo, J. Rare Earth 30 (2012) 1096–1101.
[2] B.M.E. Russbueldt, W.F. Hoelderich, J. Catal. 271 (2010) 290–304.
[3] F. Gourbilleau, L. Khomenkova, D. Bréard, C. Dufour, R. Rizk, Physica E 41 (2009) 1034–1039.
[4] N. Dhananjaya, H. Nagabhushana, B.M. Nagabhushana, B. Rudraswamy, C. Shivakumara, R.P.S. Chakradhar, J. Alloys Comp. 509 (2011) 2368–2374.
[5] R. Manigandan, K. Giribabu, R. Suresh, L. Vijayalakshmi, A. Stephen, V. Narayanan, Mater. Res. Bull. 48 (2013) 4210–4215.
[6] X. Qu, J. Dai, J. Tian, X. Huang, Z. Liu, Z. Shen, P. Wang, J. Alloys Comp. 469 (2009) 332–335.
[7] Y. Xin, Z. Wang, Y. Qi, Z. Zhang, S. Zhang, J. Alloys Comp. 507 (2010) 105–111.
[8] N. Dhananjaya, H. Nagabhushana, B.M. Nagabhushana, R.P.S. Chakradhar, C. Shivakumara, B. Rudraswamy, Physica B 405 (2010) 3795–3799.
[9] K.C. Patil, M.S. Hegde, S.T. Aruna, T. Rattan, Chemistry of Nanocrystalline Oxide Materials, Combustion Synthesis, Properties And Applications, World Scientific Publishing Co. Pvt. Ltd., UK, 2008.
[10] P. Klug, L.E. Alexander, X-ray Diffraction Procedure, Wiley, New York, 1954.
[11] G.K. Williamson, W.H. Hall, Acta Metall. 1 (1953) 22–31.
[12] B. Umesh, B. Eraiah, H. Nagabhushana, S.C. Sharma, D.V. Sunitha, B.M. Nagabhushana, J.L. Rao, C. Shivakumara, R.P.S. Chakradhar, Mater. Res. Bull. 48 (2013) 180–187.
[13] R. Hari Krishna, B.M. Nagabhushana, H. Nagabhushana, N. Suriya Murthy, S.C. Sharma, C. Shivakumara, R.P.S. Chakradhar, J. Phys. Chem. C 117 (2013) 1915–1924.
[14] W. Yang, Y. Qi, Y. Ma, X. Li, X. Guo, J. Gao, M. Chen, Mater. Chem. Phys. 84 (2004) 52–56.
[15] N. Dhananjaya, H. Nagabhushana, B.M. Nagabhushana, S.C. Sharma, B. Rudraswamy, N. Suriyamurthy, C. Shivakumara, R.P.S. Chakradhar, Appl. Phys. B 107 (2012) 503–511.
[16] L.K. Pan, Q. Sun Chang, C.M. Li, J. Phys. Chem. B 108 (2004) 3404–3406.
[17] H.Q. Cao, X.Q. Qiu, B. Luo, Y. Liang, Y.H. Zhang, R.Q. Tan, M.J. Zhao, Q.M. Zhu, Adv. Funct. Mater. 14 (2004) 243–246.
[18] B. Umesh, B. Eraiah, H. Nagabhushana, S.C. Sharma, D.V. Sunitha, B.M. Nagabhushana, C. Shivakumara, J.L. Rao, R.P.S. Chakradhar, Spectrochimica. Acta Part A 93 (2012) 228–234.
[19] B. Umesha, B. Eraiah, H. Nagabhushana, B.M. Nagabhushana, G. Nagaraja, C. Shivakumara, R.P.S. Chakradhar, J. Alloys Comp. 509 (2011) 1146–1151.
[20] N. Dilawar, S. Mahrotra, D. Varandani, B.V. Kumaraswamy, S.K. Halder, A.K. Bandyopadhyay, Mater. Charact. 59 (2008) 462–467.
[21] L.A. Tucker, F. J Karney Jr, P. McMillan, S.H. Lin, L. Lyring, Appl. Spectros. 38 (1984) 857–860.
[22] N. Dhananjaya, H. Nagabhushana, B.M. Nagabhushana, B. Rudraswamy, S.C. Sharma, D.V. Sunitha, C. Shivakumara, R.P.S. Chakradhar, Spectrosc. Chem. Acta A 96 (2012) 532–540.
[23] M. Abdullah, Khairurrijal, A. Waris, W. Sutrisno, I. Nurhasanah, A.S. Vioktalamo, Powder Technol. 183 (2008) 297–303.
[24] J.R. Cameron, N. Suntharalingam, G.N. Kenney, Thermoluminescent Dosimetry, The University of Wisconsin Press, Madison, 1968.
[25] Y.S. Horowitz, O. Avila, M. Rodriguez-Villafuerte, Nucl. Instrum. Methods. B 184 (2001) 85–112.
[26] A. Necmeddin Yazici, Mustafa Öztas, Metin Bedir, Opt. Mater. 29 (2007) 1091–1096.
[27] R. Chen, V. Pagonis, J.L. Lawless, Radia. Measur. 43 (2008) 162–166.
[28] H. Nagabhushana, Ph.D. Thesis, Bangalore University, 2003
[29] R. Chen, Y. Kirsh, Analysis of Thermally Stimulated Processes, Pergamon, New York, 1981.